New Journal of Physics
The open access journal at the forefront of physics

Deutsche Physikalische Gesellschaft DPG IOP Institute of Physics

PAPER • OPEN ACCESS

Imaging isodensity contours of molecular states with STM

To cite this article: Gaël Reecht *et al* 2017 *New J. Phys.* **19** 113033

New Journal of Physics
The open access journal at the forefront of physics

Deutsche Physikalische Gesellschaft DPG
IOP Institute of Physics

Published in partnership with: Deutsche Physikalische Gesellschaft and the Institute of Physics

OPEN ACCESS

RECEIVED
14 June 2017

REVISED
6 October 2017

ACCEPTED FOR PUBLICATION
27 October 2017

PUBLISHED
22 November 2017

PAPER

Imaging isodensity contours of molecular states with STM

Gaël Reecht[1,2], Benjamin W Heinrich[2], Hervé Bulou[1], Fabrice Scheurer[1], Laurent Limot[1] and Guillaume Schull[1]

[1] Université de Strasbourg, CNRS, IPCMS, UMR 7504, F-67000 Strasbourg, France
[2] Fachbereich Physik, Freie Universität Berlin, D-14195 Berlin, Germany

E-mail: schull@unistra.fr

Keywords: scanning tunneling microscopy, scanning tunneling spectroscopy, fulleren, C_{60}, super-atomic orbitals

Supplementary material for this article is available online

Abstract

We present an improved way for imaging the density of states of a sample with a scanning tunneling microscope, which consists in mapping the surface topography while keeping the differential conductance (dI/dV) constant. When archetypical C_{60} molecules on Cu(111) are imaged with this method, these so-called iso-dI/dV maps are in excellent agreement with theoretical simulations of the isodensity contours of the molecular orbitals. A direct visualization and unambiguous identification of superatomic C_{60} orbitals and their hybridization is then possible.

1. Introduction

The ability of the scanning tunneling microscope (STM) to image and address conductive surfaces at the atomic-scale is the main reason of its impressive success over the last three decades. Of appealing interest is the possibility of probing the density of states (DOS) of metallic or organic nanostructures adsorbed on surfaces. If the energy distribution of the sample DOS is usually directly inferred from differential conductance (dI/dV) spectra, a strict comparison requires a renormalization of the experimental data [1–5]. Measuring the spatial distribution of the DOS is even more demanding. Maps of the DOS are usually obtained by recording the dI/dV at a given target voltage (V) while keeping the tunneling current (I) constant [6–18]. However, these so-called constant-current dI/dV maps suffer from the fact that the tip–sample distance (z) varies during the scan and therefore do not properly reflect the DOS of the probed system. This well-known limitation has been evidenced for surface–confined electronic states [19, 20], adatoms [21] or molecules adsorbed on surfaces [22–24]. To extract reliable information from these maps, a time-consuming image treatment is required after acquisition [20–24].

An interesting alternative consists in recording the dI/dV while scanning the surface with an open feedback loop [21, 23–27], the so-called constant-height dI/dV mapping. In the case of a flat sample, the obtained image is an accurate representation of the DOS. However, this method is limited in the case of corrugated objects, because the effective tip–sample distance varies as a function of the (x, y) position of the tip. Moreover, since the data are acquired with a disabled feedback loop, this method requires a small thermal drift during the acquisition of the conductance map, limiting the field of application to cryogenic measurements .

In this letter, we propose a different experimental approach. It enables a direct visualization of the surface DOS that accounts for the corrugation of the sample, and which may be implemented at all working temperatures. This imaging technique consists in acquiring iso-dI/dV maps, in other words in scanning the tip across the surface while keeping the dI/dV signal constant (instead of the current) and recording changes in z. In figure 1 we provide a sketch which qualitatively shows the benefit of this approach with respect to the conventionnal constant-current and constant-height approach which fail to reproduce the spatial distribution of the DOS.

Through a combination of experiments with density functional theory (DFT) calculations, we show that the iso-dI/dV maps of non-planar C_{60} molecules on a Cu(111) surface closely reflect theoretical representations of the molecular DOS unlike standard dI/dV maps that exhibit misleading patterns for some of the C_{60} orbitals

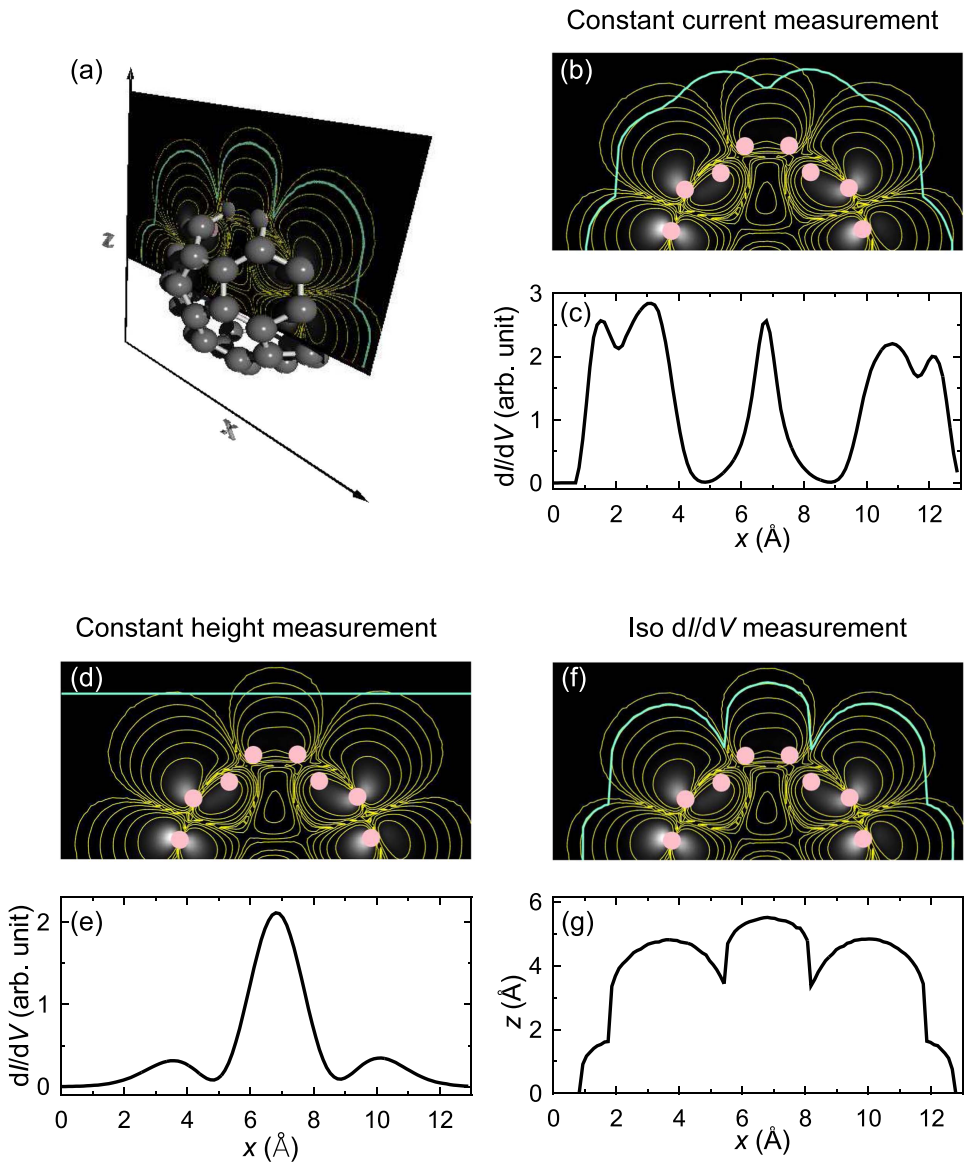

Figure 1. Illustration of the constant current, constant height and iso-dI/dV approaches. (a), (b), (d) and (f) show a (x, z) cut passing through a C_{60} molecule adsorbed on Cu(111). The position of the carbon nuclei located close (below 0.8 Å) to the (x, z) plane in (a) are indicated by white discs in (b), (d) and (f). Computed local density of states (LDOS) isocontours (from outer to inner contours: 3×10^{-6} e/bohr^3, 10^{-5} e/bohr^3, 3×10^{-5} e/bohr^3, 10^{-4} e/bohr^3, 3×10^{4} e/bohr^3, 10^{3} e/bohr^3) for the LUMO A of the C_{60} molecule (see below and supplementary material online at stacks.iop.org/NJP/19/113033/mmedia for details) appear as yellow lines. The cyan lines estimate the tip trajectory in the three different mode of measurements: in the constant current approach (b) where the trajectory is approximated by considering the sum of the two first unoccupied molecular orbitals, in the constant height approach (d), and in the iso-dI/dV approach (f). (c), (e) and (g) are the simulations of the signal of interest in the three cases: the dI/dV intensity in (c) and (e) and z in (g). In (c) and (e) the dI/dV signal is simulated by projecting the LDOS of the LUMO A on the tip trajectory. The slight asymmetry between the left and right part of (c) is an effect of the structural relaxation calculated for the C_{60} on the copper surface (see supplementary material for details).

[22]. We use this new method to provide a fresh insight into the recently reported superatomic orbitals of C_{60} monomers and dimers [10].

2. Experimental details

The experiments were performed with a STM operated at 4.6 K in UHV. Electrochemically etched W tips and Cu(111) samples were prepared by successive cycles of Ar^+ bombardment and annealing. The C_{60} molecules were sublimated from an evaporator onto the cold (≈5 K) sample. The dI/dV spectra were recorded via a lock-in amplifier by applying an AC bias of 7 kHz modulation frequency and of 10 mV rms amplitude (50 mV rms for the maps). Except for figure 2(b), the dI/dV spectra were acquired with a disabled feedback loop. To permit an unbiased comparison between the different imaging methods, the experimental maps were not processed, except for the pseudo-3D representations in figure 4, which were treated with a smoothing algorithm. All the

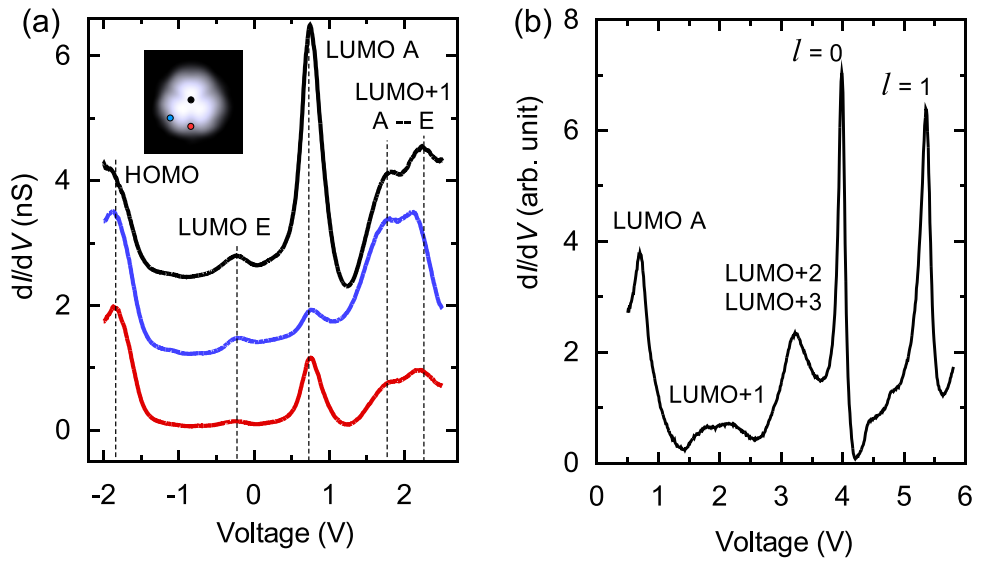

Figure 2. (a) Constant-height dI/dV spectra acquired for tip positions marked by the dots in the STM image in inset (2.3 × 2.3 nm^2, $V = 2.2$ V). (b) Constant-current dI/dV spectrum for the tip positioned above the center of C_{60} ($I = 1$ nA).

images were prepared with the Nanotec Electronica WSxM software [28]. Details of the DFT calculations are provided in the supplementary material[3].

3. Results and discussion

To start, we briefly describe the working principle of an iso-dI/dV map. At low temperature and assuming a constant tip DOS, the tunnel current can be expressed as $I(z, V) \propto \int_0^{eV} \rho_s(E)\, T(z, V, E)\, \mathrm{d}E$ [29] where ρ_s is the surface DOS and E the energy. Within the Wentzel–Kramer–Brillouin approximation, the transmission factor reads $T(z, V, E) \propto \exp(-\alpha z\sqrt{\phi + eV/2 - E})$ where ϕ is the local barrier height and $\alpha = 2\sqrt{2m}/\hbar$ (m: free electron mass, $\hbar$: reduced Planck constant). The derivative of the current with respect to V reads

$$\begin{aligned}\frac{\mathrm{d}I(z, V)}{\mathrm{d}V} &\propto e\rho_s(eV)T(z, V, eV)\\ &+\int_0^{eV} \frac{\partial T(z, V, E)}{\partial V}\rho_s(E)\,\mathrm{d}E\\ &+\int_0^{eV} \frac{\mathrm{d}z}{\mathrm{d}V}\frac{\partial T(z, V, E)}{\partial z}\rho_s(E)\,\mathrm{d}E.\end{aligned} \tag{1}$$

In the following, we disregard the third term of equation (1) as the lock-in modulation frequency of the AC bias is purposely chosen to be high compared to the time constant of the feedback loop ($\mathrm{d}z/\mathrm{d}V = 0$). We then find the usual expression [4, 21]

$$\rho_s(eV) \propto \frac{1}{eT(z, V, eV)}\left[\frac{\mathrm{d}I(z, V)}{\mathrm{d}V} + \frac{z}{4\alpha\sqrt{\phi}}I(z, V)\right], \tag{2}$$

where the second term can be neglected hereafter for usual STM conditions as discussed in detail in supplementary material (see footnote 3). Assuming that ϕ does not vary as a function of (x, y) we then write

$$z(x, y, V) \propto \ln \rho_s(x, y, eV) - c, \tag{3}$$

where $c = \ln \frac{1}{e}\frac{\mathrm{d}I(z, V)}{\mathrm{d}V}$ is a constant parameter that only depends on the dI/dV value set for the regulation, i.e., the set point. In other words, equation (3) shows that by measuring the (x, y) dependency of z it is possible to directly determine the spatial dependency of the sample DOS at a given energy eV. We stress that the level of approximation employed here is the same generally used when discussing standard dI/dV maps.

Next, to validate our imaging technique, we carry out a comparative study between standard dI/dV maps and iso-dI/dV maps by focusing our attention onto isolated C_{60} molecules on Cu(111). In the inset of figure 2(a)

[3] See supplementary material at XX for a discussion of the validity of the approximations considered in the model and for details regarding the method used to compute the electron distribution of the fullerene molecule.

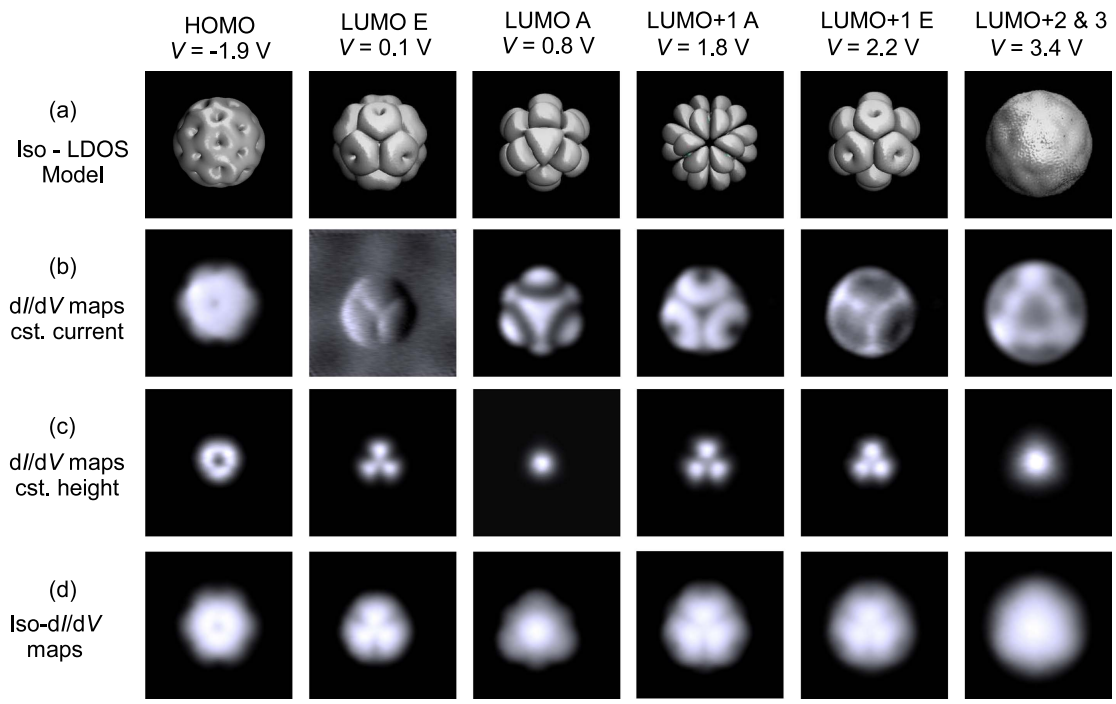

Figure 3. (a) Isosurface contours of the C_{60} orbitals computed with DFT (10^{-5} e/bohr^3). (b) Constant-current dI/dV maps ($I = 1$ nA), (c) constant-height dI/dV maps (feedback opened at $I = 1$ nA for a tip located on the center of the C_{60}) (d) iso-dI/dV maps (dI/d$V = 0.7$ nS, leading to $I \leqslant 1$ nA) of an individual C_{60} acquired at the biases identified in the spectra of figure 2. The images have the same size (3.1×3.1 nm^2).

we present a standard STM image of a C_{60} where the characteristic threefold-symmetric shape of the molecule can be recognized, indicating that it is adsorbed with a hexagon oriented towards the tip [30–32]. The dI/dV spectra (figure 2(a)) acquired for different positions of the STM tip (dots in the STM image) reveal a variety of molecular resonances. Following [33], we identify the highest occupied molecular orbital (HOMO) and the two lowest unoccupied molecular orbitals (LUMO and LUMO+1). Because of the strong interaction with the Cu(111) substrate, the LUMO and LUMO+1 orbitals are split (A and E components). The spectrum in figure 2(b) reveals further resonances at higher energy. We assign the broad peak at 3.2V to the superposition of the LUMO+2 and LUMO+3 states. The DFT calculations for the isolated, unstrained molecule reveal in fact that these states are separated by only 200 meV (see footnote 3), which is below the lifetime broadening of the molecular states (around 300 meV). Additionally, two sharp resonances appear at 4 and 5.2 V that correspond to superatomic $l = 0$ and $l = 1$ states [10], which can also be understood in the framework of whispering gallery modes [34].

Knowing the energies associated to the molecular orbitals, we can now measure their spatial distribution. To start, we display in figure 3(a) the computed LDOS isosurfaces for each molecular orbital. These gas phase DFT calculations take into account the degeneracy lifting caused by the interaction with the surface (see footnote 3). While the HOMO orbital does not split on the surface, the threefold degeneracy of the LUMO and of the LUMO +1 orbitals is partially lifted upon adsorption [22, 33]. Following simple symmetry arguments [35], we decomposed the computed LUMO and LUMO+1 orbitals into their A and E components. Since the LUMO+2 and LUMO+3 orbitals cannot be distinguished in the dI/dV spectra, we consider only the sum over the LUMO +2 and LUMO+3 isosurfaces.

Experimentally, the spatial distributions of the above orbitals have been probed following three different approaches: with constant-current dI/dV maps (figure 3(b)), constant-height dI/dV maps (figure 3(c)), and iso-dI/dV maps (figure 3(d)). The agreement between these maps and the calculated LDOS isosurfaces will be discussed separately. The constant-current dI/dV maps (figure 3(b)) agree well with the simulation for the HOMO, the LUMO A and the LUMO+1 A. At the energy of the LUMO E, the signal is very low and the pattern is asymmetric. For the E component of the LUMO+1, the constant-current dI/dV map reveals a pattern of inverted contrast compared to the calculation. This behavior, discussed in detail by Lu *et al.*, is due to variations of the tip–sample distance during the data acquisition [22]. Possible artifacts and the resulting inaccuracy of this method will be further discussed in the next section.

The dI/dV maps recorded at a constant tip height (figure 3(c)) respect the symmetry of the computed isosurfaces. However, the level of detail is reduced compared to the other approaches. More precisely, only the

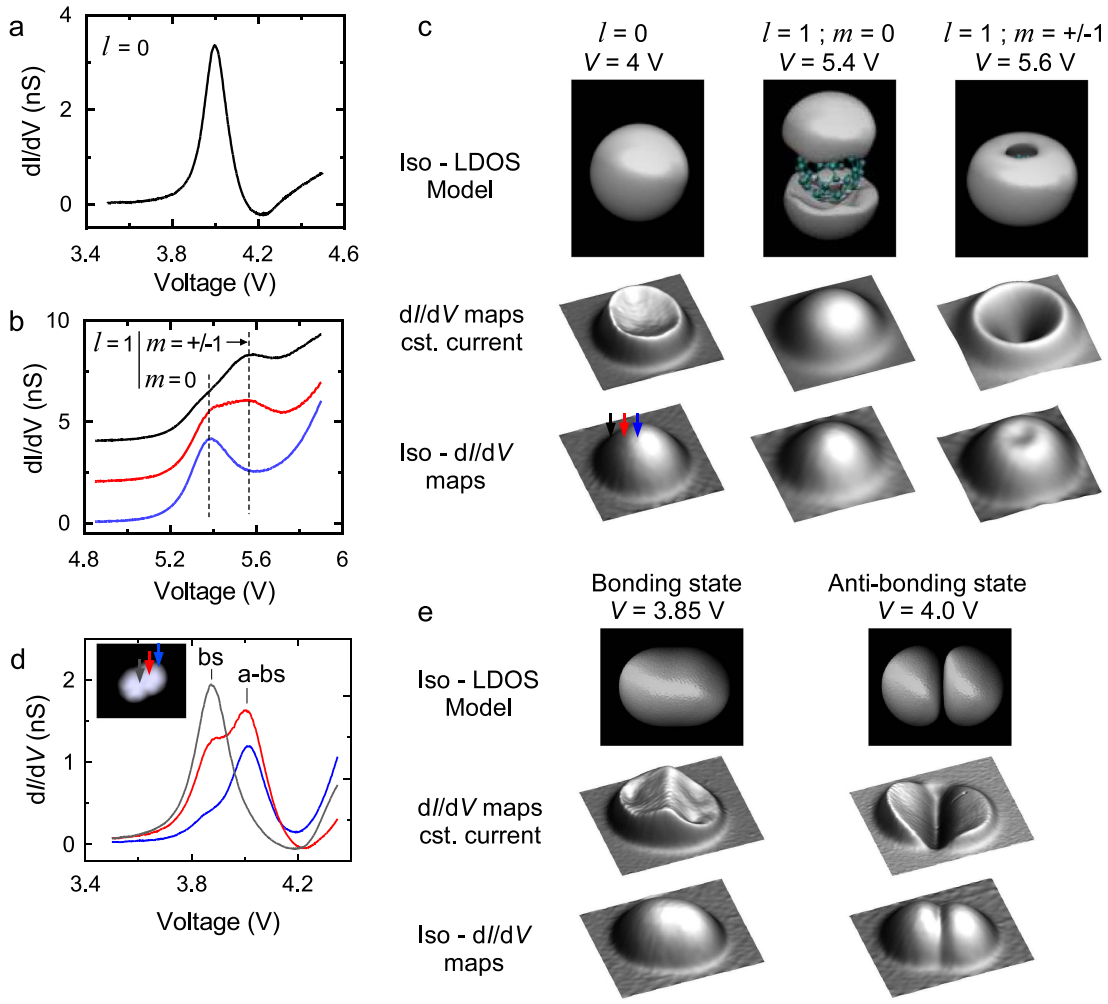

Figure 4. dI/dV spectra of (a) the $l = 0$ and (b) the $l = 1$ resonances of a single C_{60} molecule on Cu(111). The spectra in (b) were acquired for three different lateral positions of the tip with respect to the C_{60} molecule as indicated by the colored arrows in panel (c). The blue and red spectra have been offset by 2 and 4 nS, respectively (c). Computed LDOS isosurfaces (top row, 10^{-5} e/bohr^3), constant-current dI/dV maps (middle row, $I = 1$ nA for $l = 0$ and $I = 0.3$ nA for $l = 1$ maps) and iso-dI/dV maps (bottom row, dI/d$V = 0.8$ nS) of an individual C_{60} acquired at the biases identified in the spectra in (a) and (b) (size of the theoretical images: 4.0 × 5.4 nm^2 and of the experimental images: 4.0 × 4.0 nm^2). (d) dI/dV spectra acquired for three different lateral positions of the tip with respect to a C_{60} dimer as indicated by the colored arrows in the STM image in the inset of panel (d). (e) Computed LDOS isosurfaces (top row, 10^{-5} e/bohr^3), constant-current dI/dV maps (middle row, $I = 1$ nA) and iso-dI/dV maps (bottom row, dI/d$V = 0.2$ nS) for a C_{60} dimer acquired at the biases identified in the spectra in (d) (the images have the same size: 5.9 × 4.9 nm^2).

top part of the molecule is imaged. This is a direct consequence of the sphericity of C_{60}, showing that constant-height measurements produce limited results for a corrugated surface.

In contrast, the iso-dI/dV maps in figure 3(d) provide a correct representation of the spatial variation of all states. Using this method, the STM tip directly follows the LDOS isosurface of a molecular state. This largely facilitates the identification of the molecular orbitals and prevents possible misinterpretations. As an example, here we can clearly identify the LUMO A at $V = 0.8$ V, an orbital whose assignement was always uncertain in previous measurements [33] because of its similarity with the LUMO+1 E in constant-current dI/dV maps, and whose identification is not possible in constant-height maps where it only appears as a bright protrusion.

After this first proof of principle, we now use the iso-dI/dV maps to unveil the spatial distribution and composition of the resonances assigned to the $l = 0$ and $l = 1$ superatomic states. The corresponding dI/dV spectra of these states are displayed in figures 4(a) and (b), respectively. The computed LDOS isosurface for the $l = 0$ state (figure 4(c)) reveals a uniform sphere corresponding to a state fully delocalized over the C_{60} cage. While the constant-current dI/dV map exhibits a hole-like structure that would suggest a hybridization between the $l = 0$ and the $l = 1$ orbitals [10], the iso-dI/dV map is instead in perfect agreement with the theoretical predictions.

The $l = 1$ superatomic state is threefold degenerate ($m = -1, 0, 1$) in vacuum, but the dI/dV spectra acquired at different positions above the molecule on copper (see arrows in figure 4(c)) reveal instead a split resonance for this state (figure 4(b)). This suggests that the interaction with the surface lifts the degeneracy

among the m states. Our DFT computations indicate that the state at 5.4 V is associated to $m = 0$ and the state at 5.6 V to $m = \pm 1$. In figure 4(c), we present the dI/dV maps of these states along with their computed LDOS isosurfaces. Again, it can be remarked that the iso-dI/dV maps are in good agreement with calculations. The constant-current dI/dV map, instead, unsatisfactorily reproduce the $m = \pm 1$ contribution: the ring diameter is too large, the signal fall-of towards the center steep, and the signal at the center of the molecule is lower than the signal on the substrate.

The discrepancy between constant-current and iso-dI/dV maps is even more striking for a C_{60} dimer (figures 4(d) and (e)). Here, the hybridization between the $l = 0$ superatomic states of the molecules leads to a splitting of the orbital into a bonding state (bs) and an anti-bs (figure 4(d)). Contrary to constant-current dI/dV maps, the bounding and anti-bounding states can be readily visualized with iso-dI/dV maps, their pattern being self-explanatory and in perfect agreement with simulations.

4. Conclusion

To summarize, we presented a simple way to accurately map with STM the spatial variation of the DOS, which is well-suited for non-planar molecules and artificial nanostructures. Because the feedback loop is enabled during the data acquisition, our method is applicable to corrugated surfaces and in the presence of thermal drift. By imaging in this way individual C_{60} molecules on Cu(111) and comparing the results to DFT calculations, we could unambiguously identify the different resonances in the dI/dV spectra, in particular the A component of the LUMO orbital. Furthermore, we were able to correctly visualize the spatial distribution of the superatomic states in the C_{60} monomer, as well as their hybridization in the dimer case. The iso-dI/dV maps are therefore an excellent error-free alternative to commonly DOS mapping techniques employed with STM.

Acknowledgments

We thank V Speisser, J-G Faullumel and M Romeo for technical support. The Agence National de la Recherche (Grant No. ANR-14-CE26-0016-01, ANR-15-CE09-0017, ANR-13-BS10-0016, ANR-10-LABX-0026 CSC, ANR-11-LABX-0058 NIE) and the International Center for Frontier Research in Chemistry are acknowledged for financial support. This work was performed using HPC resources from GENCI-IDRIS (Grant No. 2016097459). BWH gratefully acknowledges funding by the Deutsche Forschungsgemeinschaft through Grant HE7368/2.

ORCID iDs

Guillaume Schull https://orcid.org/0000-0002-4205-0431

References

[1] Stroscio J A, Feenstra R M and Fein A P 1986 Electronic structure of the Si(111)2 × 1 surface by scanning-tunneling microscopy *Phys. Rev. Lett.* **57** 2579–82
[2] Ukraintsev V A 1996 Data evaluation technique for electron-tunneling spectroscopy *Phys. Rev.* B **53** 11176
[3] Wagner C, Franke R and Fritz T 2007 Evaluation of $i(v)$ curves in scanning tunneling spectroscopy of organic nanolayers *Phys. Rev.* B **75** 235432
[4] Koslowski B, Dietrich C, Tschetschetkin A and Ziemann P 2007 Evaluation of scanning tunneling spectroscopy data: approaching a quantitative determination of the electronic density of states *Phys. Rev.* B **75** 035421
[5] Passoni M, Donati F, Li Bassi A, Casari C S and Bottani C E 2009 Recovery of local density of states using scanning tunneling spectroscopy *Phys. Rev.* B **79** 045404
[6] Hasegawa Y and Avouris P 1993 Direct observation of standing wave formation at surface steps using scanning tunneling spectroscopy *Phys. Rev. Lett.* **71** 1071–4
[7] Wang K, Zhao J, Yang S, Chen L, Li Q, Wang B, Yang S, Yang J, Hou J G and Zhu Q 2003 Unveiling metal-cage hybrid states in a single endohedral metallofullerene *Phys. Rev. Lett.* **91** 185504
[8] Nilius N, Wallis T M and Ho W 2005 Tailoring electronic properties of atomic chains assembled by STM *Appl. Phys.* A **80** 951–6
[9] Temirov R, Soubatch S, Luican A and Tautz F S 2006 Free-electron-like dispersion in an organic monolayer film on a metal substrate *Nature* **444** 350–3
[10] Feng M, Zhao J and Petek H 2008 Atomlike, hollow-core-bound molecular orbitals of C_{60} *Science* **320** 359–62
[11] Schull G, Néel N, Becker M, Krüger J and Berndt R 2008 Spatially resolved conductance of oriented C_{60} *New J. Phys.* **10** 065012
[12] Schull G, Frederiksen T, Brandbyge M and Berndt R 2009 Passing current through touching molecules *Phys. Rev. Lett.* **103** 206803
[13] Auwärter W *et al* 2010 Site-specific electronic and geometric interface structure of Co-tetraphenyl-porphyrin layers on Ag(111) *Phys. Rev.* B **81** 245403
[14] Müllegger S *et al* 2011 Preserving charge and oxidation state of Au(111) ions in an agent-functionalized nanocrystal model system *ACS Nano* **5** 6480–6
[15] Ruffieux P *et al* 2012 Electronic structure of atomically precise graphene nanoribbons *ACS Nano* **6** 6930–5

[16] Fahrendorf S, Atodiresei N, Besson C, Caciuc V, Matthes F, Blügel S, Kögerler P, Bürgler D E and Schneider C M 2013 Accessing 4f-states in single-molecule spintronics *Nat. Commun.* **4** 2425
[17] Nacci C, Ample F, Bleger D, Hecht S, Joachim C and Grill L 2015 Conductance of a single flexible molecular wire composed of alternating donor and acceptor units *Nat. Commun.* **6** 8397
[18] Pham V D, Repain V, Chacon C, Bellec A, Girard Y, Rousset S, Smogunov A, Dappe Y J and Lagoute J 2016 Control of molecule-metal interaction by hydrogen manipulation in an organic molecule *J. Phys. Chem. Lett.* **7** 1416
[19] Hörmandinger G 1994 Imaging of the Cu(111) surface state in scanning tunneling microscopy *Phys. Rev.* B **49** 13897–905
[20] Li J, Schneider W-D and Berndt R 1997 Local density of states from spectroscopic scanning-tunneling-microscope images: Ag(111) *Phys. Rev.* B **56** 7656
[21] Ziegler M, Néel N, Sperl A, Kröger J and Berndt R 2009 Local density of states from constant-current tunneling spectra *Phys. Rev.* B **80** 125402
[22] Lu X, Grobis M, Khoo K H, Louie S G and Crommie M F 2003 Spatially mapping the spectral density of a single C_{60} molecule *Phys. Rev. Lett.* **90** 096802
[23] Krenner W, Kühne D, Klappenberger F and Barth J V 2013 Assessment of scanning tunneling spectroscopy modes inspecting electron confinement in surface-confined supramolecular networks *Sci. Rep.* **3** 1454
[24] Zhang Y *et al* 2015 Low-temperature scanning tunneling microscopy study on the electronic properties of a double-decker DyPc2 molecule at the surface *Phys. Chem. Chem. Phys.* **17** 27019–26
[25] Heinrich B W, Iacovita C, Brumme T, Choi D-J, Limot L, Rastei M V, Hofer W A, Kortus J and Bucher J-P 2010 Direct observation of the tunneling channels of a chemisorbed molecule *J. Phys. Chem. Lett.* **1** 1517–23
[26] Reecht G, Bulou H, Scheurer F, Speisser V, Carrière B, Mathevet F and Schull G 2013 Oligothiophene nanorings as electron resonators for whispering gallery modes *Phys. Rev. Lett.* **110** 056802
[27] Söde H, Talirz L, Gröning O, Pignedoli C A, Berger R, Feng X, Müllen K, Fasel R and Ruffieux P 2015 Electronic band dispersion of graphene nanoribbons via fourier-transformed scanning tunneling spectroscopy *Phys. Rev.* B **91** 045429
[28] Horcas I, Fernandez R, Gomez-Rodriguez J M, Colchero J, Gomez-Herrero J and Baro A M 2007 Wsxm: a software for scanning probe microscopy and a tool for nanotechnology *Rev. Sci. Instrum.* **78** 013705
[29] Simmons J G 1963 Generalized formula for the electric tunnel effect between similar electrodes separated by a thin insulating film *J. Appl. Phys.* **34** 1793–803
[30] Larsson J A, Elliott S D, Greer J C, Repp J, Meyer G and Allenspach R 2008 Orientation of individual C_{60} molecules adsorbed on Cu(111): low-temperature scanning tunneling microscopy and density functional calculations *Phys. Rev.* B **77** 115434
[31] Heinrich B W, Rastei M V, Choi D-J, Frederiksen T and Limot L 2011 Engineering negative differential conductance with the Cu(111) surface state *Phys. Rev. Lett.* **107** 246801
[32] Shin H *et al* 2014 Structure and dynamics of C_{60} molecules on Au(111) *Phys. Rev.* B **89** 245428
[33] Silien C, Pradhan N A, Ho W and Thiry P A 2004 Influence of adsorbate-substrate interaction on the local electronic structure of C_{60} studied by low-temperature STM *Phys. Rev.* B **69** 115434
[34] Reecht G, Bulou H, Schull G and Scheurer F 2016 Single molecules as whispering galleries for electrons *J. Phys.: Condens. Matter* **28** 165001
[35] Hands I D, Dunn J L and Bates C A 2010 Calculation of images of oriented C_{60} molecules using molecular orbital theory *Phys. Rev.* B **81** 205440